Nanoparticle Separation

DOI: 10.1002/ange.201209504

Bypassing the Limitations of Classical Chemical Purification with DNA-Programmable Nanoparticle Recrystallization**

*Matthew R. Jones and Chad A. Mirkin**

Crystallization is a common and invaluable tool in chemistry for obtaining compounds with a high degree of purity. In a mixture of two or more species, conditions are found in which the desired component is able to selectively form a crystalline structure that excludes impurity species which are unable to incorporate into the ordered lattice formed by the product. This process has been used to purify myriad organic molecules, resolve racemic mixtures with chiral additives, and even separate complex protein mixtures to arrive at samples of maximum homogeneity.[1] Without such tools to obtain materials that are uniform in their structure, function, and composition, elucidation of their chemical and physical properties would be extremely challenging and, in some cases, impossible. Interestingly, a host of anisotropic nanoparticle syntheses currently suffer from an analogous problem as the aforementioned molecular systems—the presence of impurity nanostructures with disparate shapes that obviate a variety of measurements, confound data analysis, and preclude potential applications.[2] Surprisingly few separation methods exist for addressing this challenge[3] and it has been shown that conventional methods for crystallizing nanoparticles based on drying effects or capillary forces are not effective at separating differently shaped nanoparticles.[4] However, recent work from our group has demonstrated that anisotropic nanostructures functionalized with a dense shell of oligonucleotides are capable of hybridizing one another and forming ordered superlattices with a binding constant six orders of magnitude larger than comparable spherical nanoparticle conjugates.[5] In addition, the programmability inherent to DNA in both sequence and length allows the interactions between nanoparticles to be tailored to optimize their assembly into crystalline superlattices. Herein we show that DNA-programmable nanoparticle crystallization is capable of maximizing the thermodynamic selectivity for one particle shape to form an ordered phase in preference to another. This is in stark contrast to classical chemical crystallization in which the molecular interactions that dictate crystal formation are predetermined by the species being purified and are essentially unalterable. The preferential formation of ordered superlattices that exclude impurity nanoparticles of undesired shapes allows the crystallized nanoparticle product to be separated, resulting in samples of substantially increased homogeneity (Scheme 1). Finally, we show the first experimental derivation of molar extinction coefficients for these materials, as determination of this property requires a degree of sample purity which has been previously unobtainable.

[*] Prof. C. A. Mirkin
Department of Chemistry, Materials Science & Engineering and International Institute for Nanotechnology
Northwestern University
2145 Sheridan Road, Evanston, IL 60208-3113 (USA)
E-mail: chadnano@northwestern.edu

M. R. Jones
Department of Materials Science & Engineering
Northwestern University (USA)

[**] C.A.M. acknowledges the following awards for support of this work: AFOSR FA9550-09-1-0294, FA9550-11-1-0275 and FA9550-12-1-0280, DoD/NSSEFF/NPS N00244-09-1-0012 and N00244-09-1-0071, NSF MRSEC DMR-1121262, and the DoE/Office of Science/Office of Basic Energy Sciences NERC DE-SC0000989. M.R.J. is grateful to the NSF for a Graduate Research Fellowship and to Northwestern University for a Ryan Fellowship. Small-angle X-ray scattering was carried out at the DuPont-Northwestern-Dow Collaborative Access Team (DND-CAT) beamline located at Sector 5 of the Advanced Photon Source (APS). DND-CAT is supported by E. I. DuPont de Nemours & Co., The Dow Chemical Company, and the State of Illinois. Use of the APS was supported by US Department of Energy, Office of Science, Office of Basic Energy Sciences, under Contract No. DE-AC02-06CH11357. The ICP-AES analysis was completed at the Northwestern University Integrated Molecular Structure Education and Research Center (IMSERC).

Supporting information for this article is available on the WWW under http://dx.doi.org/10.1002/anie.201209504.

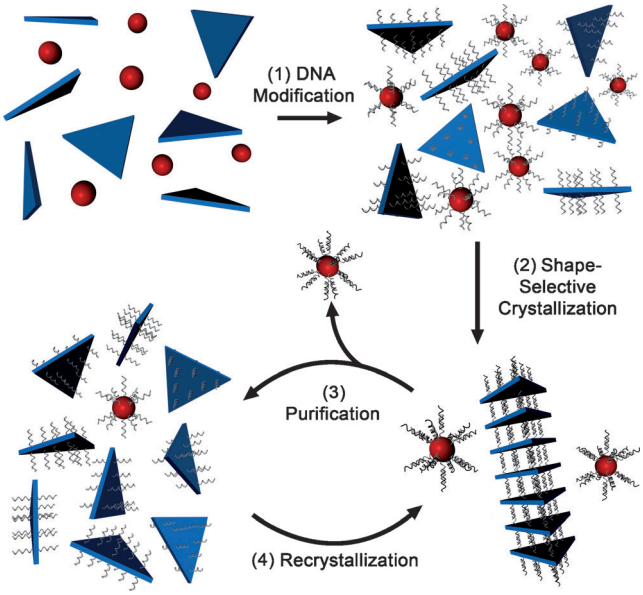

Scheme 1. DNA-programmable nanoparticle crystallization. After DNA functionalization of all the particles (1), anisotropic structures can be selectively crystallized into ordered superlattices (2), which facilitates their removal from impurity species (3). Additional rounds of purification (4) results in samples with improved purity.

Previously, we and others have observed that gold nanoparticles functionalized with alkylthiol modified oligonucleotides exhibit a variety of unexpected properties,[6] some of which include high cellular uptake without transfection agents,[7] resistance to enzymatic DNA degradation,[8] and the ability to assemble into extremely well-ordered superlattices according to straightforward design rules.[5,9] Of particular interest is the discovery that DNA-functionalized nanoparticles exhibit a 100-fold increase in binding constant for the hybridization of complementary oligonucleotides.[10] The observation that DNA–nanoparticle conjugates exhibit enhanced binding constants has already been used to sort mixtures of spherical nanoparticles of different diameters on the basis of their size.[11] However, this approach is limited by the relatively weak dependence of binding constant on sphere size, and did not result in the formation of ordered nanoparticle phases owing to the lack of understanding of the importance of weak DNA interactions in facilitating the formation of well-defined crystals at the time. The recent demonstration that nanoparticle shape can induce directional assembly interactions and change conjugate binding to complementary NPs by a factor of several million lays the foundation for the crystallization approach used herein.[5,12]

The problem of particle non-uniformity in the field of nanoscience has been recognized as a major challenge since, unlike molecules, nanostructures have rarely been synthesized in an atomically pure fashion, yet their properties are heavily dependent on the number of atoms in the material.[13] This issue is compounded for anisotropic particles as the property of shape becomes an additional variable that must be regulated with a high degree of precision. Herein, the gold triangular nanoprism synthesis is used as a model system because nanoprisms are considerably under-represented in both fundamental and applied studies of nanoparticles, owing in part to the challenge of their separation from concomitantly generated spherical particle impurities.[2b] Despite this difficulty, triangular nanoprisms have been recognized as appealing nanostructures because of their unique shape and complex optical resonances,[2b,14] but have been featured in notably fewer reports than other established anisotropic structures.[15] For comparison, single-crystalline gold nanorods, which can be synthesized naturally with high purity (ca. 98%),[16] have deservingly enjoyed a high degree of success in studies of both fundamental scientific relevance[17] and those focused on applied systems ranging from optical data storage[18] to biological therapeutics.[19]

As with most seed-mediated nanoparticle syntheses,[20] triangular nanoprisms (sometimes referred to as prisms for brevity) can be made in a size-controlled manner by changing the concentration of spherical seed nanoparticles added to a growth solution. For prisms (see Supporting Information for experimental details), this strategy allows for edge lengths to be tailored from 200 to less than 20 nm (thickness remains constant at ca. 7 nm), all while maintaining a polydispersity of 10% or less (Supporting Information, Table S1). This notable degree of edge-length control also allows for a highly tunable optical response across the visible and near-infrared regions of the electromagnetic spectrum (peak values range from 600 to over 1300 nm; Figure 1a), as the surface plasmon resonance (SPR) for anisotropic noble-metal nanoparticles is heavily dependent on the aspect ratio of the structure.[20,21] Although this synthetic method is appealing as it results in a solution of high-quality triangular nanoprisms, it also generates an excess of spherical nanoparticle impurities; in a typical synthesis, nanoprisms constitute only 20–30% of all particles while spheres make up the remainder (SPR peak at ca. 530 nm; Figure 1a,b). Moreover, while increasing the seed concentration decreases the nanoprism edge length, it also decreases the diameter of the spherical particles generated (Figure S1). For example, a synthesis of 100 nm edge-length nanoprisms produces spherical impurities of 34 nm diameter, while a synthesis of 50 nm edge-length nanoprisms produces spheres with a diameter of 25 nm (Figure 1c). The commensurate nature of the prism and sphere sizes, regardless of the seed concentration used, makes segregation of the two species particularly challenging; all attempts to purify the prisms by centrifugation or filtration result in little to no differential separation.

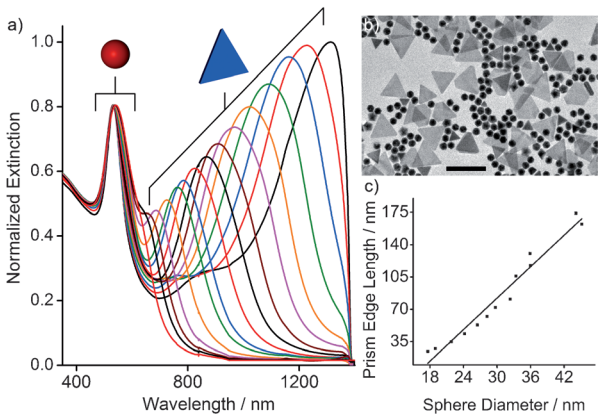

Figure 1. a) Extinction spectra from a range of as-synthesized nanoprisms with redshifting plasmon resonances corresponding to increasing prism edge lengths ($\lambda_{max} \approx 600$ to 1300 nm). The peak at approximately 530 nm corresponds to spherical impurities and is present in every synthesis. b) TEM image of a typical synthesis showing a mixture of prisms and spheres; scale bar is 200 nm. c) Linear relationship between the prism edge length and sphere diameter generated by a synthesis with a particular seed concentration.

To investigate the ability for DNA-functionalization to facilitate purification through a selective crystallization mechanism, as-synthesized mixtures of prisms and spheres were functionalized with oligonucleotide ligands according to literature precedents.[12,22] To induce interparticle association, linker oligonucleotides were introduced that were designed with two functional regions, one which hybridizes the nanoparticle-bound strands, and another that presents a short self-complementary "sticky end" overhang at the periphery of the nanostructures (see Supporting Information for sequences). These sticky end sequences, while individually weak, collectively facilitate a relatively strong association between particles through numerous DNA linkages.[5,12] Importantly, because these oligonucleotides primarily consist of duplexed structures, they are sufficiently rigid so as to preserve the shape of the nanoparticles to which they are attached, thus allowing any preferences for crystallization of a particular

nanoparticle shape to be most pronounced. In other words, ligands that are too flexible will cause particles to appear more spherical from a hydrodynamic perspective and destroy any shape-dependent effects. Upon addition of linker strands to mixtures of DNA-functionalized prisms and spheres, an immediate color change was observed, followed by visible aggregation over the course of several minutes indicating a DNA-mediated association process, consistent with previous results.[5,6,22]

To determine the feasibility of purification by crystallization, a DNA-mediated nanoparticle hybridization analysis was conducted to follow the assembly process under thermodynamic control. After the addition of linker oligonucleotides, as-prepared mixtures of prisms and spheres were heated to 55 °C to dehybridize all the DNA connections and then slowly cooled to 10 °C while simultaneously monitoring the SPR of each particle shape (spheres ca. 530 nm, prisms 600–1300 nm depending on size, Figure 1 a). Because interparticle association results in large shifts in the SPR wavelength and intensity, the hybridization transition temperature (T_m) can be determined independently for each nanoparticle species from this experiment.[23] At high temperatures, both species are dispersed and exhibit their maximum SPR extinction (Figure 2 a). Upon cooling, a dramatic drop in the extinction of the particles indicates interparticle association. For a representative set of particles, the nanoprisms hybridize one another at temperatures 10 °C higher than their spherical particle contaminants, indicating a considerable thermodynamic selectivity for particle shape (Figure 2 a). It is important to note that although the results presented in Figure 2 are for a combination of 60 nm edge-length prisms and 27 nm spheres, the same qualitative behavior in association temperature was observed for a range of prism/sphere combinations generated by the synthesis (Figure S2). Recent work from our group suggests that the origin of this separation in transition temperature arises from the confinement of DNA ligands on the flat, faceted surfaces of anisotropic nanostructures.[5]

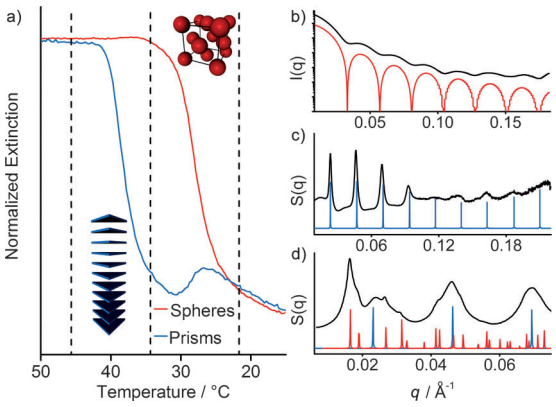

Figure 2. a) Extinction at SPR peak monitored as a function of temperature for an as-prepared solution of DNA-modified 60 nm edge-length prisms and 27 nm spheres. The sharp drop denotes the thermodynamic onset of interparticle association (insets indicate the ordered phases that form for each nanoparticle shape). b–d) Small angle X-ray scattering patterns taken at temperatures indicated by the dashed lines in (a) with experimental results shown in black and modeled results shown in red or blue. b) Form-factor at high temperatures indicating a majority population of non-interacting spherical particles (model for perfect 27 nm spheres shown in red). c) Structure-factor at intermediate temperatures indicating the presence of lamellar nanoprism superlattices (model for perfect lamellar superlattices composed of 60 nm edge-length prisms is shown in blue). d) Structure-factor at low temperatures indicating both FCC spherical nanoparticle superlattices and lamellar nanoprism superlattices (model for perfect FCC superlattices shown in red and perfect lamellar superlattices shown in blue).

To explore the importance of DNA design on the behavior of the system, prism and sphere hybridization temperatures were determined using several different oligonucleotide linkers. Sticky end sequences were designed to vary in strength and to minimize base-pair slippage effects.[24] Thermodynamic data were collected using a synthesis of 40 nm edge-length prisms with 22 nm spheres, as these two particles become functionalized with the same number of DNA strands and therefore allow an accurate comparison to be made based solely on nanoparticle shape.[5] As a function of the Gibbs free energy of a particular sticky end sequence,[25] several important trends can be observed (Table 1). As expected, the absolute transition temperatures decrease as the driving force for hybridization becomes weaker. More interestingly, the prism transition temperature has a weaker dependence on the sticky end interaction strength than the sphere transition temperature. This result originates from the greater degree of multivalency in the face-to-face interactions of prisms than with the curved surfaces of spheres.[5] The consequence of this effect is that the separation between prism and sphere transition temperatures (ΔT_m) is maximized for weak linkers. This ability to differentially modulate the association strength between nanoparticle species highlights a major advantage of using a DNA-based approach to nanoparticle crystallization.

Table 1: Hybridization temperatures (T_m) for a combination of 40 nm edge-length prisms and 22 nm spheres varying the linker sticky end strength.

Sticky end sequence[a]	$\Delta G°$ [kcal mol^{-1}][b]	T_m Prism [°C]	T_m Sphere [°C]	ΔT_m [°C]
GAGCTC	−5.75	50.85	49.68	1.17
TAGCTA	−4.26	41.67	38.48	3.19
TCTAGA	−4.04	36.42	32.90	3.51
TGCA	−3.52	32.45	28.26	4.19

[a] Sequences are listed 5′ to 3′ and represent the terminal overhang bases only. [b] Values were calculated using the model described in Ref. [25] with one initiation parameter and both symmetry and salt corrections.

While these results strongly imply the ability to preferentially crystallize prisms over spheres at the appropriate temperature, monitoring of the plasmon shift is unable to differentiate a random aggregation process from one in which ordered phases are formed. To interrogate the presence and evolution of long-range order upon cooling of the system, small angle X-ray scattering (SAXS) data were collected at relevant temperatures indicated by the hybridization results (dashed lines Figure 2 a; see Supporting Information for details of the SAXS analysis and modeling). At high temper-

atures, an oscillatory form factor indicative of the absence of long-range order was observed (Figure 2b). This scattering pattern was best modeled by the form factor of a solution primarily containing spherical particles, as expected from the extinction spectra and TEM results (Figure 1). Scattering patterns obtained at intermediate temperatures, however, showed strong periodic structure factor indicative of a lamellar ordering of particles (Figure 2c). A modeled pattern for a one-dimensional superlattice of nanoprisms showed excellent agreement with the experiment and is consistent with previous observations.[12] Upon further cooling, scattering peaks corresponding to FCC order were observed overlaid with those arising from one-dimensional lamellar order (Figure 2d). A modeled scattering pattern consisting of a two-phase mixture of FCC spherical nanoparticle superlattices and lamellar nanoprism superlattices showed excellent agreement with the data. These results confirm that nanoprisms indeed associate and form a crystalline nanoparticle superlattice phase preferentially over spherical impurity particles.

Having confirmed the feasibility of preferentially crystallizing prisms over spheres, we next sought to exploit the considerable difference in transition temperature as a means of purification. As-prepared mixtures of DNA-functionalized prisms and spheres were heated to 55 °C and then cooled to temperatures between the two hybridization transitions so that only nanoprisms could form an ordered crystalline phase (middle dashed line, Figure 2a). After annealing samples under these conditions for 12 h to several days, visible phase separation was observed in the form of a large pellet with a bright red supernatant. After mild centrifugation, the supernatant could be removed without disturbing the pellet and on analysis was found to contain extinction peaks indicative of a solution of spherical particles with no nanoprisms (Figure 3a). Likewise, re-dispersion of the pellet in water resulted in a blue or green solution, depending on particle size, and was found to exhibit extinction peaks indicative of a solution of triangular nanoprisms with no spherical particle impurities (Figure 3a). TEM images of the as-prepared solution, supernatant, and re-dispersed pellet confirmed the spectroscopic data and indicated the separation of each species to be extremely efficient (Figure 3b–d). Indeed, image analysis of approximately 2000 particles revealed a purity of over 95% after a single separation step; this corresponds to a separation factor of 76 (Figure S3).[26] Interestingly, just as for the crystallization of molecular species, nanoparticle product can be crystallized and purified sequentially several times to arrive at samples of improved quality. Using this approach, nanoprisms that were recrystallized an additional two times accounted for approximately 99% of the total number of particles, a remarkable degree of purity, particularly for anisotropic nanostructures. In addition, this crystallization strategy can be used to refine the dispersity of solutions containing a distribution of prism sizes, as larger nanoprisms will exhibit higher hybridization transition temperatures than smaller prisms (Figure S2). The ability to simultaneously improve both the purity and monodispersity of nanoparticle samples highlights the versatility of the DNA-based crystallization approach described herein.

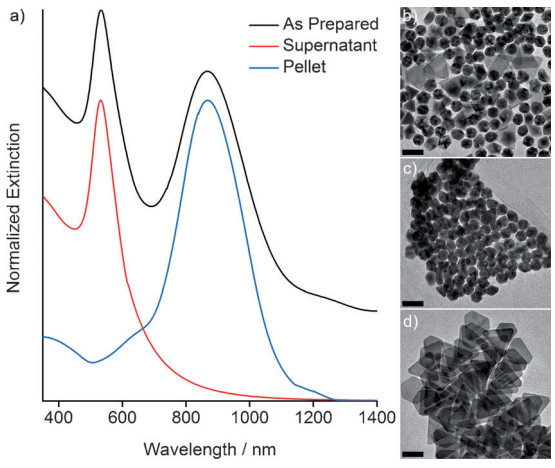

Figure 3. a) Extinction spectra of an as-prepared mixture of prisms and spheres, separated spherical nanoparticle impurities found in the supernatant and purified nanoprism product found in the re-dispersed pellet (as-prepared curve is offset for clarity). b–d) TEM images of b) the mixed nanoparticle solution, c) the spherical particle supernatant, and d) the re-dispersed nanoprism pellet; scale bars are 50 nm.

As in the case of traditional organic chemistry, purity of a desired compound is unavoidably linked to the ability to probe its chemical and physical properties. An excellent example of this for nanoparticle systems is quantification of their size-dependent molar extinction coefficients, as determination of both the absolute extinction of a solution of particles and the number of particles in that solution can be confounded by the presence of impurity nanostructures. While empirical extinction coefficients have been determined for both spherical nanoparticles and nanorods owing to their inherent synthetic purity,[27] the lack of such uniformity in solutions of triangular nanoprisms has been a major barrier to the derivation of their extinction coefficients. To overcome this limitation, DNA-programmable nanoparticle crystallization was used to purify a range of nanoprism sizes, allowing for spectroscopically pure samples of particles as small as approximately 30 nm to be generated (Figure 4a). Inductively coupled plasma atomic emission spectroscopy (ICP-AES) was then used to determine atomic gold content of dilutions of known extinction values for each nanoprism size (Figure S4). Using particle dimensions determined from TEM, linear interpolations of absolute extinction versus nanoparticle concentration allowed for derivation of the molar extinction coefficient as a function of the size of the nanoprism (Figure 4b; see Supporting Information for experimental details). For comparison, the size-dependent molar extinction coefficients of spherical particles and nanorods of several different dimensions are provided from empirical studies found in the literature.[27] Interestingly, when evaluating these shapes on the basis of nanostructure volume, the nanoprisms are shown to be more efficient at interacting with resonant light than nearly all the other structures, and they do so over a wide range of particle sizes. This illustrates that triangular nanoprisms are ideal nanostructures for maximizing plasmonic light–matter interactions on an atom-by-atom basis.

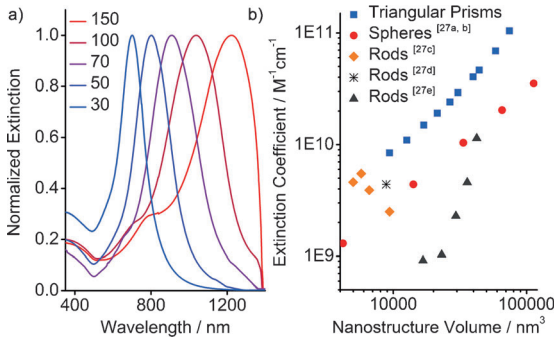

Figure 4. a) Extinction spectra of a range of nanoprism sizes separated from their spherical impurities by crystallization. Nanoprism edge lengths are denoted in nanometers. b) Log–Log plot of the size-dependent molar extinction coefficients of a variety of gold nanoparticles. All quantities have been plotted against the volume of the nanostructure so as to allow for comparison between different shapes. Values obtained for triangular nanoprisms are derived from a concentration-dependent ICP-AES analysis while values for all other particles are obtained from literature. Triangular nanoprisms are 7 nm in thickness and range in edge length from 40 to 130 nm; spheres (Refs [27a,b]) range in diameter from 20 to 60 nm; rods (Ref [27c]) range in diameter from 12 to 18 nm and range in length from 36 to 53 nm; rods (Ref [27d]) are 15 nm in diameter and 50 nm in length; rods (Ref [27e]) are 25 nm in diameter and range in length from 34 to 86 nm.

In conclusion, we have shown that the programmable nature of DNA-mediated nanoparticle interactions allows crystallization/recrystallization to be used to generate samples of exceptional purity without being bound by the limitations of conventional molecular crystallization. Using this approach, triangular nanoprism samples can now be generated with purities of 95% or greater across a broad range of particle sizes. In addition, the uniformity of these samples has allowed for the first determination of molar extinction coefficients as a function of size which reveal a marked advantage of nanoprisms over several other common nanostructures on the basis of maximizing the efficiency of light–matter interactions. These results, therefore, have considerable relevance to both the nanoparticle and plasmonics communities, which depend heavily on samples of optimal homogeneity for a variety of applications and optical investigations.

Received: November 27, 2012
Published online: February 13, 2013

Keywords: crystallization · DNA · nanoparticles · plasmonics · purification

[1] a) R. J. Fessenden, J. Fessenden, S. P. Feist, *Organic Laboratory Techniques*, 3rd ed., Brooks/Cole, Pacific Grove, CA, **2001**; b) H. E. Zaugg, *J. Am. Chem. Soc.* **1955**, *77*, 2910–2910; c) A. S. Myerson, K. Toyokura in *ACS Symposium Series*, *Vol. 438*, American Chemical Society, Washington, DC, **1990**.

[2] a) N. R. Jana, L. Gearheart, C. J. Murphy, *J. Phys. Chem. B* **2001**, *105*, 4065–4067; b) J. E. Millstone, S. Park, K. L. Shuford, L. Qin, G. C. Schatz, C. A. Mirkin, *J. Am. Chem. Soc.* **2005**, *127*, 5312–5313; c) M. Liu, P. Guyot-Sionnest, *J. Phys. Chem. B* **2005**, *109*, 22192–22200; d) T. K. Sau, C. J. Murphy, *J. Am. Chem. Soc.* **2004**, *126*, 8648–8649; e) Y. Sun, Y. Xia, *Science* **2002**, *298*, 2176–2179; f) F. Kim, S. Connor, H. Song, T. Kuykendall, P. Yang, *Angew. Chem.* **2004**, *116*, 3759–3763; *Angew. Chem. Int. Ed.* **2004**, *43*, 3673–3677; g) M. L. Personick, M. R. Langille, J. Zhang, N. Harris, G. C. Schatz, C. A. Mirkin, *J. Am. Chem. Soc.* **2011**, *133*, 6170–6173.

[3] a) K. Park, H. Koerner, R. A. Vaia, *Nano Lett.* **2010**, *10*, 1433–1439; b) B. P. Khanal, E. R. Zubarev, *J. Am. Chem. Soc.* **2008**, *130*, 12634–12635; c) S. R. Beeram, F. P. Zamborini, *ACS Nano* **2010**, *4*, 3633–3646; d) G.-T. Wei, F.-K. Liu, C. R. C. Wang, *Anal. Chem.* **1999**, *71*, 2085–2091; e) V. Sharma, K. Park, M. Srinivasarao, *Proc. Natl. Acad. Sci. USA* **2009**, *106*, 4981–4985; f) L. Bai, X. Ma, J. Liu, X. Sun, D. Zhao, D. G. Evans, *J. Am. Chem. Soc.* **2010**, *132*, 2333–2337; g) O. Akbulut, C. R. Mace, R. V. Martinez, A. A. Kumar, Z. Nie, M. R. Patton, G. M. Whitesides, *Nano Lett.* **2012**, *12*, 4060–4064.

[4] a) E. V. Shevchenko, D. V. Talapin, N. A. Kotov, S. O'Brien, C. B. Murray, *Nature* **2006**, *439*, 55–59; b) P. J. Yunker, T. Still, M. A. Lohr, A. G. Yodh, *Nature* **2011**, *476*, 308–311.

[5] M. R. Jones, R. J. Macfarlane, A. E. Prigodich, P. C. Patel, C. A. Mirkin, *J. Am. Chem. Soc.* **2011**, *133*, 18865–18869.

[6] a) C. A. Mirkin, R. L. Letsinger, R. C. Mucic, J. J. Storhoff, *Nature* **1996**, *382*, 607–609; b) J. I. Cutler, E. Auyeung, C. A. Mirkin, *J. Am. Chem. Soc.* **2012**, *134*, 1376–1391.

[7] N. L. Rosi, D. A. Giljohann, C. S. Thaxton, A. K. R. Lytton-Jean, M. S. Han, C. A. Mirkin, *Science* **2006**, *312*, 1027–1030.

[8] D. S. Seferos, A. E. Prigodich, D. A. Giljohann, P. C. Patel, C. A. Mirkin, *Nano Lett.* **2008**, *9*, 308–311.

[9] a) R. J. Macfarlane, B. Lee, M. R. Jones, N. Harris, G. C. Schatz, C. A. Mirkin, *Science* **2011**, *334*, 204–208; b) S. Y. Park, A. K. R. Lytton-Jean, B. Lee, S. Weigand, G. C. Schatz, C. A. Mirkin, *Nature* **2008**, *451*, 553–556; c) D. Nykypanchuk, M. M. Maye, D. van der Lelie, O. Gang, *Nature* **2008**, *451*, 549–552; d) R. J. Macfarlane, M. R. Jones, A. J. Senesi, K. L. Young, B. Lee, J. Wu, C. A. Mirkin, *Angew. Chem.* **2010**, *122*, 4693–4696; *Angew. Chem. Int. Ed.* **2010**, *49*, 4589–4592; e) E. Auyeung, J. I. Cutler, R. J. Macfarlane, M. R. Jones, J. Wu, G. Liu, K. Zhang, K. D. Osberg, C. A. Mirkin, *Nat. Nanotechnol.* **2012**, *7*, 24–28.

[10] A. K. R. Lytton-Jean, C. A. Mirkin, *J. Am. Chem. Soc.* **2005**, *127*, 12754–12755.

[11] J.-S. Lee, S. I. Stoeva, C. A. Mirkin, *J. Am. Chem. Soc.* **2006**, *128*, 8899–8903.

[12] M. R. Jones, R. J. Macfarlane, B. Lee, J. Zhang, K. L. Young, A. J. Senesi, C. A. Mirkin, *Nat. Mater.* **2010**, *9*, 913–917.

[13] K. Suzuki, S. Sato, M. Fujita, *Nat. Chem.* **2010**, *2*, 25–29.

[14] a) J. E. Millstone, S. J. Hurst, G. S. Métraux, J. I. Cutler, C. A. Mirkin, *Small* **2009**, *5*, 646–664; b) J. E. Millstone, G. S. Métraux, C. A. Mirkin, *Adv. Funct. Mater.* **2006**, *16*, 1209–1214; c) K. L. Shuford, M. A. Ratner, G. C. Schatz, *J. Chem. Phys.* **2005**, *123*, 114713; d) K. L. Kelly, E. Coronado, L. L. Zhao, G. C. Schatz, *J. Phys. Chem. B* **2002**, *107*, 668–677; e) J. E. Millstone, W. Wei, M. R. Jones, H. Yoo, C. A. Mirkin, *Nano Lett.* **2008**, *8*, 2526–2529.

[15] a) M. R. Jones, J. E. Millstone, D. A. Giljohann, D. S. Seferos, K. L. Young, C. A. Mirkin, *ChemPhysChem* **2009**, *10*, 1461–1465; b) M. J. Banholzer, N. Harris, J. E. Millstone, G. C. Schatz, C. A. Mirkin, *J. Phys. Chem. C* **2010**, *114*, 7521–7526; c) D. A. Walker, K. P. Browne, B. Kowalczyk, B. A. Grzybowski, *Angew. Chem.* **2010**, *122*, 6912–6915; *Angew. Chem. Int. Ed.* **2010**, *49*, 6760–6763; d) D. A. Walker, C. E. Wilmer, B. Kowalczyk, K. J. M. Bishop, B. A. Grzybowski, *Nano Lett.* **2010**, *10*, 2275–2280; e) K. L. Young, M. R. Jones, J. Zhang, R. J. Macfarlane, R. Esquivel-Sirvent, R. J. Nap, J. Wu, G. C. Schatz, B. Lee, C. A. Mirkin, *Proc. Natl. Acad. Sci. USA* **2012**, *109*, 2240–2245.

[16] a) B. Nikoobakht, M. A. El-Sayed, *Chem. Mater.* **2003**, *15*, 1957 – 1962; b) X. Huang, S. Neretina, M. A. El-Sayed, *Adv. Mater.* **2009**, *21*, 4880 – 4910.
[17] a) H. Wang, T. B. Huff, D. A. Zweifel, W. He, P. S. Low, A. Wei, J.-X. Cheng, *Proc. Natl. Acad. Sci. USA* **2005**, *102*, 15752 – 15756; b) A. M. Funston, C. Novo, T. J. Davis, P. Mulvaney, *Nano Lett.* **2009**, *9*, 1651 – 1658.
[18] P. Zijlstra, J. W. M. Chon, M. Gu, *Nature* **2009**, *459*, 410 – 413.
[19] a) X. Huang, I. H. El-Sayed, W. Qian, M. A. El-Sayed, *J. Am. Chem. Soc.* **2006**, *128*, 2115 – 2120; b) S. E. Lee, G. L. Liu, F. Kim, L. P. Lee, *Nano Lett.* **2009**, *9*, 562 – 570; c) A. Wijaya, S. B. Schaffer, I. G. Pallares, K. Hamad-Schifferli, *ACS Nano* **2008**, *3*, 80 – 86.
[20] a) Y. Xia, Y. Xiong, B. Lim, S. E. Skrabalak, *Angew. Chem.* **2009**, *121*, 62 – 108; *Angew. Chem. Int. Ed.* **2009**, *48*, 60 – 103.
[21] M. R. Jones, K. D. Osberg, R. J. Macfarlane, M. R. Langille, C. A. Mirkin, *Chem. Rev.* **2011**, *111*, 3736 – 3827.
[22] J. E. Millstone, D. G. Georganopoulou, X. Xu, W. Wei, S. Li, C. A. Mirkin, *Small* **2008**, *4*, 2176 – 2180.
[23] a) S. K. Ghosh, T. Pal, *Chem. Rev.* **2007**, *107*, 4797 – 4862; b) R. Jin, G. Wu, Z. Li, C. A. Mirkin, G. C. Schatz, *J. Am. Chem. Soc.* **2003**, *125*, 1643 – 1654; c) J. J. Storhoff, A. A. Lazarides, R. C. Mucic, C. A. Mirkin, R. L. Letsinger, G. C. Schatz, *J. Am. Chem. Soc.* **2000**, *122*, 4640 – 4650.
[24] H. D. Hill, S. J. Hurst, C. A. Mirkin, *Nano Lett.* **2008**, *9*, 317 – 321.
[25] J. SantaLucia, *Proc. Natl. Acad. Sci. USA* **1998**, *95*, 1460 – 1465.
[26] E. B. Sandell, *Anal. Chem.* **1968**, *40*, 834 – 835.
[27] a) P. Mulvaney, M. Giersig, A. Henglein, *J. Phys. Chem.* **1992**, *96*, 10419 – 10424; b) S. Link, M. A. El-Sayed, *J. Phys. Chem. B* **1999**, *103*, 8410 – 8426; c) C. J. Orendorff, C. J. Murphy, *J. Phys. Chem. B* **2006**, *110*, 3990 – 3994; d) H. Liao, J. H. Hafner, *Chem. Mater.* **2005**, *17*, 4636 – 4641; e) Values obtained from documentation accompanying commercially available nanorods (Nanopartz Inc.).

